Journal of Nanobiotechnology

RESEARCH

Open Access

CD44-targeting hyaluronic acid-selenium nanoparticles boost functional recovery following spinal cord injury

Wenqi Luo[1†], Yueying Li[2†], Jianhui Zhao[1], Renrui Niu[1], Chunyu Xiang[1], Mingyu Zhang[1], Chunsheng Xiao[3], Wanguo Liu[1*] and Rui Gu[1*]

Abstract

Background Therapeutic strategies based on scavenging reactive oxygen species (ROS) and suppressing inflammatory cascades are effective in improving functional recovery after spinal cord injury (SCI). However, the lack of targeting nanoparticles (NPs) with powerful antioxidant and anti-inflammatory properties hampers the clinical translation of these strategies. Here, CD44-targeting hyaluronic acid-selenium (HA-Se) NPs were designed and prepared for scavenging ROS and suppressing inflammatory responses in the injured spinal cord, enhancing functional recovery.

Results The HA-Se NPs were easily prepared through direct reduction of seleninic acid in the presence of HA. The obtained HA-Se NPs exhibited a remarkable capacity to eliminate free radicals and CD44 receptor-facilitated internalization by astrocytes. Moreover, the HA-Se NPs effectively mitigated the secretion of proinflammatory cytokines (such as IL-1β, TNF-α, and IL-6) by microglia cells (BV2) upon lipopolysaccharide-induced inflammation. In vivo experiments confirmed that HA-Se NPs could effectively accumulate within the lesion site through CD44 targeting. As a result, HA-Se NPs demonstrated superior protection of axons and neurons within the injury site, leading to enhanced functional recovery in a rat model of SCI.

Conclusions These results highlight the potential of CD44-targeting HA-Se NPs for SCI treatment.

Keywords CD44 targeting, Inflammation, Reactive oxygen species, Selenium nanoparticles, Spinal cord injury

Introduction

Spinal cord injury (SCI) is a catastrophic condition that results in severe disability, including paraplegia or quadriplegia, and gives rise to a range of serious multi-system complications, such as recurrent bladder and kidney infections, intestinal problems, as well as cardiac and respiratory dysfunction, placing a heavy burden on individuals, families, and society [1, 2]. In clinical practice, the conventional approaches for treating SCI encompass administration of high-dose methylprednisolone, implementation of surgical interventions aimed at stabilizing and decompressing the spinal cord, and provision of rehabilitative therapy [3, 4]. However, currently available therapies are mainly palliative and do not offer substantial functional recovery [5–8]. Hence, there is an impetus

[†]Wenqi Luo and Yueying Li contributed equally to this work.

*Correspondence:
Wanguo Liu
liuwanguo6016@jlu.edu.cn
Rui Gu
gurui@jlu.edu.cn
[1] Department of Orthopaedic Surgery, China-Japan Union Hospital of Jilin University, Changchun 130033, People's Republic of China
[2] Department of Hand and Foot Surgery, China-Japan Union Hospital of Jilin University, Changchun 130033, People's Republic of China
[3] Key Laboratory of Polymer Ecomaterials, Changchun Institute of Applied Chemistry, Chinese Academy of Sciences, Changchun 130022, People's Republic of China

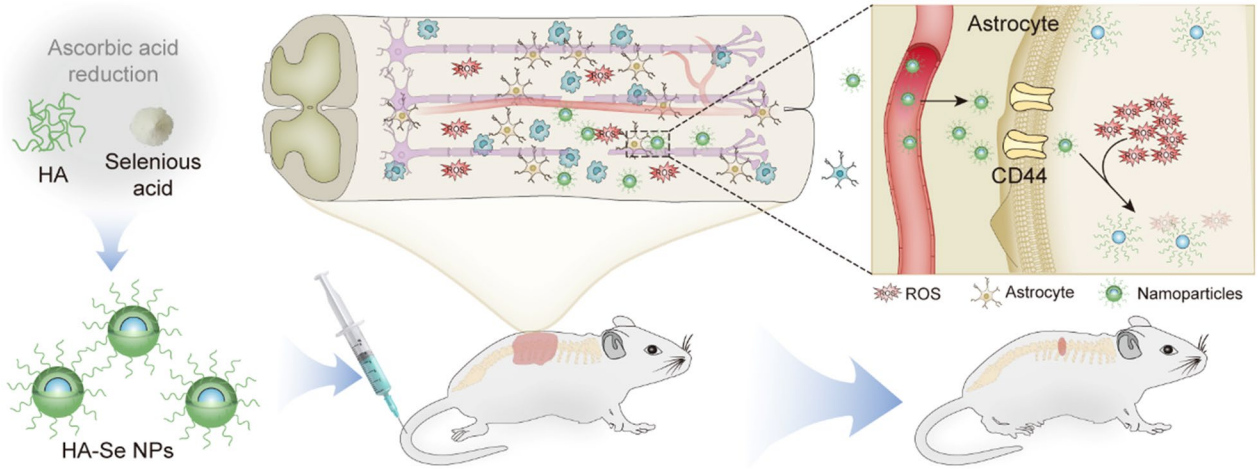

Scheme 1 Schematic illustration of the preparation of CD44-targeting HA-Se NPs for promoting functional recovery after SCI

to explore alternative therapeutic strategies that consider the pathophysiology of SCI. The deleterious pathophysiological events that occur following SCI are the consequence of a biphasic process that encompasses both primary and secondary impairments [9–12]. The primary damage stems from the mechanical force and the initial impairment that subsequently initiates a rapidly escalating sequence of degenerative occurrences, commonly referred to as the secondary injury [13–15]. The secondary injury comprises various pathological events, such as the generation of reactive oxygen species (ROS) and the occurrence of inflammation [16–18]. In particular, overproduction of ROS at the injury site leads to the depletion of endogenous antioxidants and the disruption of redox balance, causing extensive damage to intracellular biomacromolecules, such as DNA and proteins, followed by consequent neuronal cell death [17, 19]. Moreover, excess ROS provoke an aggravated inflammatory response, recruiting and activating inflammatory cells, such as microglia and astrocytes, which further exacerbates neuronal cell death [14, 17]. Hence, it can be argued that ROS significantly contribute to the occurrence and progression of secondary injury in SCI.

It is well-documented that timely therapeutic intervention through ROS scavenging and inflammation suppression at the initial phase of SCI can significantly improve neurological and functional recuperation [14, 18, 20–23]. Recently, the utilization of nano-biomaterials as a therapeutic approach for SCI has garnered considerable interest [5, 15, 24–26]. Among them, selenium (Se)-based nanoparticles (NPs) have emerged as promising candidates due to their capacity for scavenging ROS and mitigating inflammation [27–29]. It has been proven that Se supplementation can forestall ROS accumulation, suppress lipid peroxidation, and prevent cellular damage [30–33]. Moreover, Se has been shown to mitigate functional deficits in the central nervous system due to its antioxidation properties [15, 34, 35]. Notwithstanding, conventional Se NPs have drawbacks, such as limited targeting ability, substandard stability, and limited solubility, which impede their application in basic research and the clinic [36]. It is therefore imperative to formulate innovative approaches to ensure the accumulation of Se NPs at the lesion site, favorable biological effects, and safety for therapeutic applications.

Hyaluronic acid (HA), a polysaccharide originating from the natural extracellular matrix, serves as a ligand for cluster of differentiation 44 (CD44) receptor [37]. Furthermore, it has been demonstrated that HA is beneficial for repairing spinal cord tissue by preventing the formation of glial scars [38]. In the current work, we focused the engineering and fabrication of HA-stabilized selenium nanoparticles (HA-Se NPs) specifically targeting the overexpressed CD44 receptor within the injured spinal cord, with the aim of mitigating secondary injury (Scheme 1). The HA-Se NPs were prepared via reduction of seleninic acid in the presence of sodium ascorbate. The obtained HA-Se NPs exhibited an exceptional ROS scavenging ability. Moreover, in vivo assessments confirmed that the HA-Se NPs tended to accumulate at the injury site through active binding to CD44, which is upregulated in activated astrocytes. By virtue of these targeting and ROS-scavenging abilities, the HA-Se NPs achieved superior neuroprotection and enhanced functional recovery in a rat model of SCI.

Materials and methods

High-molecular-weight HA (with a molecular weight of 2×10^5 g mol^{-1}) and seleninic acid were procured from Huaxia Chemical Reagent Co., Ltd. (Chengdu, China). Sodium ascorbate was obtained from Aladdin Bio-Chem Technology Co., Ltd. (Shanghai, China). Dulbecco's modified Eagle's medium (DMEM) and fetal bovine serum were purchased from Gibco (Thermo Fisher Scientific, Waltham, MA, USA). 3-(4,5-dimethyl-thiazol-2-yl)-2,5-diphenyl tetrazolium bromide (MTT), 2′,7′-dichlorodihydrofluorescein diacetate (DCFH-DA; D6883), and 4′,6-diamidino-2-phenylindole dihydrochloride (DAPI) were purchased from Sigma-Aldrich (St. Louis, MO, USA). Hydrogen peroxide solution (30 wt% in water) was obtained from Sinopharm Chemical Reagent Co., Ltd. 1,1-Diphenyl-2-picrylhydrazyl (DPPH) was purchased from Shanghai Macklin Biochemical Co., Ltd. Anti-GFAP, anti-NF200, and anti-NeuN primary antibodies were obtained from Abcam (Cambridge, UK). Anti-CD44 and anti-caspase-3 antibodies were purchased from Cell Signaling Technology (Danvers, MA, USA). The dialysis membrane was obtained from Greenbird Technology Co., Ltd (Shanghai, China). The remaining compounds were obtained from commercial providers and used without any further manipulation.

Preparation and characterization of HA-Se NPs

Briefly, 45 mL of aqueous HA solution (1.5 mg/mL) was mixed with 600 µL of seleninic acid (0.1 M) in a round-bottom flask. Subsequently, 3 mL of ascorbic acid aqueous solution (0.1 M) was gradually introduced into the mixture with constant stirring at ambient temperature (~22 °C). The gradual addition of sodium ascorbate solution resulted in a noticeable alteration of the solution's color from a clear hue to a red tint. Upon completion of the reaction, the mixture was subjected to dialysis for 48 h using ultrapure water and a dialysis bag with a molecular weight cutoff (MWCO) of 300 kDa. Thereafter, the solution was centrifuged at 4,000 rpm for 20 min. Finally, the HA-Se NPs were obtained via lyophilization as red powder (yield: 82.5%).

The size and zeta potential of HA-Se nanoparticles were evaluated via dynamic light scattering on a Malvern Zetasizer Nano ZS (ZEN3600, Malvern Instruments, Worcestershire, UK). The morphology of HA-Se NPs was observed through transmission electron microscopy (TEM) (JOEL-1011, Tokyo, Japan) at an accelerating voltage of 200 kV and emission-scanning electron microscopy (SEM) (Zeiss, Oberkochen, Germany). Using the KBr pellet method, Fourier transform infrared spectra (FT IR) were recorded with a Win-IR device (Bio-Rad Laboratories, Hercules, CA, USA). The amount of selenium in HA-Se NPs was determined using an inductively coupled plasma mass spectrometer (ICP-MS, Xseries II, Thermo Scientific, USA). The antioxidant capacity of HA-Se NPs was explored by analyzing their influence on DPPH free radicals. In the control group, a combination of water (2 mL) and DPPH anhydrous ethanol solution (0.4 mM, 2 mL) was utilized. The experimental group, on the other hand, included HA-Se NPs (250/1, 000 µg/mL, 2 mL) and DPPH anhydrous ethanol solution (0.4 mM, 2 mL), while the blank group included HA-Se NPs (250/1,000 µg/mL, 2 mL) and absolute ethanol (2 mL). The background was modified through the utilization of a mixture of 2 mL of water and 2 mL of anhydrous ethanol. The aforementioned groups were exposed to darkness for a period of 30 min, after which the absorbance at 517 nm was recorded on a Bio-Rad 680 microplate reader (TECAN Trading AG, Switzerland). The free radical-scavenging rate (%) was determined as per the following formula: $(1-(A_{\text{experimental}} - A_{\text{blank}})/A_{\text{control}}) \times 100$, where $A_{experimental}$, A_{blank}, and $A_{control}$ represent the absorbance values of the experimental, blank, and control group, respectively.

Cytotoxicity and neuroprotective activity assay in vitro

Astrocytes, pheochromocytoma 12 (PC12) cells, and the BV2 microglia cell line were procured from the Cell Bank of the Chinese Academy of Science (Shanghai, China). The MTT method was employed to evaluate the cytotoxicity of HA-Se NPs in astrocytes and PC12 cells [22]. In brief, astrocytes or PC12 cells were seeded onto 96-well plates at a concentration of 8,000 cells per well and incubated for 12 h in DMEM medium. Subsequently, different concentrations of HA-Se NPs were added to the wells, ranging from 3.125 to 100 µg/mL. Control group cells were subjected to treatment with phosphate-buffered saline (PBS). Three parallel tests were carried out for every concentration. After a further incubation for either 24 or 48 h, solution containing 5 mg/mL MTT was added to each well at a volume of 20 µL and allowed to incubate for a further 4 h. Thereafter, the medium was discarded and exchanged with 150 µL of dimethyl sulfoxide. The absorbance of each well at 492 nm was determined using an absorbance microplate reader (Infinite M200, Tecan, Switzerland). In an effort to assess the potential protective properties of HA-Se NPs against H_2O_2-induced oxidative stress [22], astrocytes were grown in 96-well plates, with each well containing 8,000 cells. Prior to H_2O_2 exposure, the cells underwent 30-min pre-treatment with either PBS or HA-Se NPs at 50 and 100 µg/mL. Thereafter, the cells were exposed to 100 µM H_2O_2 for 24 h, and their viability was assessed via MTT assay. To further evaluate cell viability, we employed a commercial live-dead cell staining kit from Sigma-Aldrich. After staining, cells were observed through a confocal laser-scanning

microscope (CLSM) (LSM 780, Zeiss). Dead cells were then quantified using the ImageJ software (1.51k, NIH, Bethesda, MD, USA). DCFH-DA fluorescence intensity was measured to quantitatively determine ROS levels in both astrocytes and PC12 cells.

Assessment of proinflammatory cytokine levels in vitro and in vivo

In order to examine the capacity of HA-Se NPs to inhibit inflammation, BV2 cells were first seeded onto 6-well plates at a density of 2×10^5 cells/well and permitted to settle for 12 h. Cells were then subjected to pre-treatment with either PBS or HA-Se NPs (20 μg/mL) for 2 h. Thereafter, the cells were exposed to 1 μg/mL lipopolysaccharide (LPS) for 24 h. To determine the levels of interleukin (IL)-1β, tumor necrosis factor α (TNF-α), and IL-6, we employed commercially available enzyme-linked immunosorbent assay kits (Anoric Bio-technology Co., Ltd) and an absorbance microplate reader (Infinite M200, Tecan, Switzerland). The assays were performed in triplicate. To confirm the in vivo suppressive effects of HA-Se NPs on inflammatory cells, which typically exhibit a peak at the lesion site within 3–7 days post-injury, immunofluorescence analysis of spinal cord tissue samples was carried out using anti-CD68 and anti-Iba-1 antibodies.

Animal model of SCI

Approval for animal procedures was granted by the Animal Ethics Committee of Jilin University (approval No. SY202103013). Female Sprague-Dawley rats, aged 6–8 weeks, were procured from Liaoning Changsheng Biotechnology Ltd. and provided with *ad libitum* access to food and water. Sprague-Dawley rats were anesthetized via intraperitoneal administration of pentobarbital sodium intraperitoneally at a dose of 5 mg per kilogram of body weight. After disinfecting with iodine volts, a T10 laminectomy procedure was performed to reveal the spinal cord, and the injury model was established using a weight-drop device (C4P01-001, Shenzhen, China). A 40-g rod was allowed to fall from a height of 50 mm, making contact with the spinal cord's uncovered dorsal surface, and causing an initial depth of penetration of 2.5 mm. Following the surgical intervention, the fascia, muscle, and skin were sequentially closed in layers. The Sprague-Dawley rats were housed in a temperature-regulated setting at 25 ± 2 °C and were provided with ad libitum access to both water and food. Moreover, the Sprague-Dawley rats were treated with cefazolin, given twice daily for a duration of 5 days at a dose of 25 mg/kg. The urinary bladders of Sprague-Dawley rats were manually emptied twice daily until they regained the ability to urinate autonomously.

The SCI rats were randomly divided into four groups ($n=9$). The rats were treated with saline, HA-Se NPs (1 mg kg^{-1}), HA-Se NPs (5 mg kg^{-1}), or HA-Se NPs (10 mg kg^{-1}). All rats received intravenous injections. The animals underwent anesthesia and were then perfused with 4% paraformaldehyde and PBS at the 12-week interval post-injury. After being harvested from the center of injury, the spinal cords, which had a length of roughly 2 cm, were treated with a 4% paraformaldehyde solution. Thereafter, the specimens were embedded in paraffin for further analysis. These sections were employed in subsequent experiments.

Analysis of CD44 expression

CD44 expression in the spinal cord was evaluated seven days after injury. The tissue slices underwent dual labeling using a primary anti-CD44 antibody in conjunction with primary anti-glial fibrillary acidic protein (GFAP), anti-NeuN, anti-CD68, or anti-Iba-1 antibodies. For immunofluorescence staining, the antibody utilized is documented in Additional file 1: Table S1 . CLSM was utilized to obtain images. Immunofluorescence experiments were performed three times. To examine the potential for inflammation to stimulate CD44 expression in astrocytes, the cells were grown on 6-well plates and subjected to varying concentrations of LPS (10, 20, or 40 μg/mL) or glutamate (100, 200, or 400 μM) for a duration of 24 h. CD44 expression was evaluated via western blot and immunofluorescence analyses. Following LPS activation for 24 h, astrocytes were rinsed with PBS and were then fixed with 4% PFA. Nonspecific binding sites were obstructed using blocking buffer for a period of 1.5 h. Thereafter, the cells were incubated with an anti-CD44 primary antibody and incubated overnight at a temperature of 4 °C. After being washed with PBS, the cells were exposed to secondary antibodies and incubated for a duration of 2 h at room temperature. Another PBS wash was then carried out, and the cells were subsequently exposed to 1,1′-dioctadecyl-3,3,3′,3′-tetramethylindocarbocyanine perchlorate (Dil), a fluorescent probe for cell membranes, for a duration of 15 min. Ultimately, the astrocytes were examined and visualized via CLSM. This experiment was also repeated three times.

To ascertain the potential association between the CD44 receptor and the absorption of HA-Se NPs, a competitive cellular uptake experiment was performed. Following a 24-h incubation with LPS, astrocytes were subjected to a 4-h pretreatment with either HA (1 mg/mL) or PBS. Samples were then subjected to incubation with 0.1 mg/mL HA-Se NPs for 4 and 8 h, followed by five washes with PBS and fixation with 4% PFA for a period of 20 min. Cell nuclei were stained with DAPI staining prior

to observation via confocal microscopy (LSM 780, Zeiss, Germany). Mean intracellular fluorescence intensity was determined using ImageJ (1.51k, NIH, Bethesda, MD, USA).

Biodistribution of HA-Se NPs

NH_2-Cy5-labeled HA-Se NPs were synthesized as previously described [39]. To visualize the in vivo biodistribution of HA-Se NPs, rats were administered Cy5-labeled HA-Se NPs at a dose of 10 mg/kg subsequent to the injury. At specific intervals (4, 12, and 24 h), the rats were humanely sacrificed, and their primary organs (heart, lung, liver, spleen, brain, kidney, and spinal cord) were obtained. Control samples were obtained by administering Cy5-labeled HA-Se NPs to sham rats, which were then euthanized 12 h post-injection. The obtained organs were imaged and analyzed using a Maestro In Vivo Imaging System (IVIS Lumina LT Series III, PerkinElmer, USA).

Behavioral analysis of SCI rats

The Basso, Beattie, Bresnahan (BBB) locomotor rating scale was employed to evaluate the motor functions of rats. Based on the 21-point BBB open-field grading scale, rats were individually assessed in an open field for 5 min. The BBB score assesses the voluntary movements of rat limbs through a scale of 0 to 21. A score of 0 represents paralysis, whereas 21 indicates normal movements. Evaluation was performed by two separate evaluators, and the marks were ascertained through mutual accord.

Histological and immunofluorescence analyses

Fixed spinal cord samples were embedded in paraffin, followed by sectioning into 4 μm thick slices in the coronal plane. Through H&E staining, pathological changes, which included enlargement of cavity area and inflammatory cell infiltration, were investigated. The extent of demyelination was determined by staining spinal cord slices from each group with 0.1% Luxol fast blue (LFB) at the 12-week mark following injury.

To evaluate the myelin sheath ultrastructure, we prepared tissue for transmission electron microscopy (TEM) as per our previously established method [22]. The spinal cord segments were fixed overnight at a temperature of 4 °C using 2.5% glutaraldehyde. Thereafter, the segments were sliced into 1 mm^3 pieces, osmicated for 90 min, and then dehydrated for a period of 135 min. Subsequently, the ultrathin sections were subjected to staining with uranyl acetate and lead citrate, followed by a thorough examination using TEM. To assess the expression of neurofilament 200 (NF200) and NeuN, the slices were first subjected to permeation with a PBS solution that contained 0.1% Triton X-100 for a period of 15 min. Thereafter, a 2-h incubation period with 5% bovine serum albumin (BSA) was utilized for blocking, followed by thorough washing with PBS containing 0.2% Tween 20. Subsequently, the portions were subjected to an overnight incubation at a temperature of 4 °C, utilizing primary antibodies against NF200 and NeuN. The axons and neurons were distinguished using anti-NF200 and anti-NeuN, respectively. Additional file 1: Table S1 provides details on antibody dilution for immunofluorescence. Images were acquired through CLSM. The potential toxicity of HA-Se NPs was assessed 12 weeks post-treatment through H&E staining of vital organs.

Western blotting

Spinal cord tissue was lysed using a buffer solution that contained proteinase inhibitors. The lysate was then centrifuged at 13,300 rpm for 15 min. Protein concentration was determined using a BCA protein kit (Beyotime, Shanghai, China). The procedure involved separation of 10 μg protein from each sample using sodium dodecyl sulfate-polyacrylamide gel electrophoresis (SDS-PAGE) and subsequent transfer of the separated protein onto polyvinylidenedifluoride (PVDF) membranes (EMD Millipore, Billerica, MA, USA). For blocking, the membranes were treated with 5% bovine serum albumin for 1.5 h. Thereafter, membranes were incubated with either anti-CD44 or anti-caspase-3 antibodies at 4 °C overnight. After washing, the membranes were incubated with a secondary antibody conjugated to horseradish peroxidase for 2 h at room temperature. Target protein expression was normalized based on that of GAPDH or β-actin. Western blotting antibody data is available in Additional file 1: Table S2. An enhanced chemiluminescence Western blot detection system (AI600 Imager; GE Healthcare, Chicago, IL, USA) was used to capture protein bands. Densitometric analysis of the protein bands was carried out using Multi Gauge software (Fuji, Tokyo, Japan). Western blotting experiments were repeated three times.

Statistical analysis

To determine the statistical significance of differences, a one-way analysis of variance or t-tests were performed utilizing Prism 8.0.2 (GraphPad Software, San Diego, CA, USA). $^{*}P < 0.05$ was deemed statistically significant. $^{**}P < 0.01$ and $^{***}P < 0.001$ were deemed highly significant.

Results

Preparation and characterization of HA-Se NPs

The synthesis of HA-Se NPs was accomplished through a straightforward reduction reaction, utilizing water-soluble HA as a stabilizing and capping agent [40]. The HA acts as a capping agent to facilitate NP formation and also provides a protective shell to prevent NP aggregation.

The HA-Se NPs exhibited a size of 101.2 ± 1.4 nm and a polydispersity index of 0.17 ± 0.02 (Fig. 1A). The particle size of HA-Se NPs did not change significantly over a period of 3 days (Additional file 1: Figure S1), which indicates a high degree of stability. Through TEM, we observed that HA-Se NPs possessed a core-shell structure, with a diameter averaging roughly 95 nm (Fig. 1B and Additional file 1: Figure S2). Moreover, SEM analysis revealed that HA-Se NPs exhibited a uniform spherical morphology, with an approximate size of 94 nm (Fig. 1C). The zeta potential of HA-Se NPs was −26.2 ± 0.47. Their composition was investigated in greater detail using X-ray photoelectron spectroscopy, which confirmed that the nanoparticles were predominantly composed of carbon, nitrogen, oxygen, and selenium, as indicated by the distinctive peaks detected in the C 1s, N 1s, O 1s, and Se 3d spectra. (Additional file1: Figure S3). The selenium content of HA-Se NPs was 10.8%, as determined via ICP-MS. As oxidative stress can cause significant and continuous harm to the central area and adjacent spinal cord [6, 24], the capacity of HA-Se NPs to eliminate ROS was subsequently examined. HA-Se NPs exhibited remarkable ability in eliminating DPPH free radicals that was concentration- and exposure duration-dependent, as shown in Fig. 1D.

Biocompatibility of HA-Se NPs, protection from H_2O_2-induced oxidative stress, and inflammation suppression in vitro

The biocompatibility of the synthesized HA-Se NPs was investigated through MTT tests. The impact of HA-Se NPs on astrocytes and PC12 cells was evaluated through observation and analysis after 24 or 48 h of exposure at concentrations ranging from 0 to 100 mg/L. Notwithstanding the highest concentration tested, the HA-Se NPs induced no apparent cytotoxicity, as shown in Additional file 1: Figure S4. Oxidative stress occurs when excessive ROS are generated after SCI [41–43]. HA-Se NPs successfully protected astrocytes from oxidative stress induced by H_2O_2, preventing cell death (Figure S5). Live/dead cell staining further confirmed the protective effect of HA-Se NPs (Fig. 2A, B and Additional file 1:

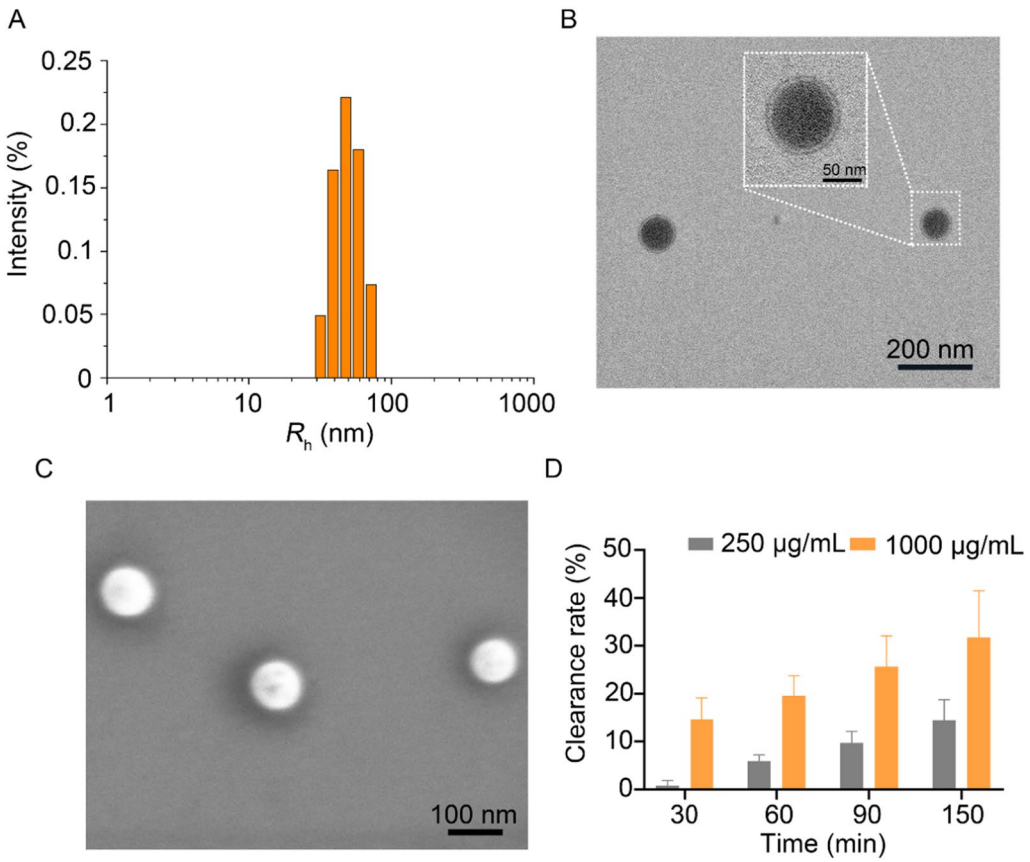

Fig. 1 Characterization of hyaluronic acid-selenium nanoparticles (HA-Se NPs). **A** Dynamic light scattering measurement of HA-Se NPs. **B** Transmission and **C** scanning electron microscopy imaging of HA-Se NPs. **D** The efficacy of HA-Se NPs in scavenging free radicals was evaluated at varying concentrations

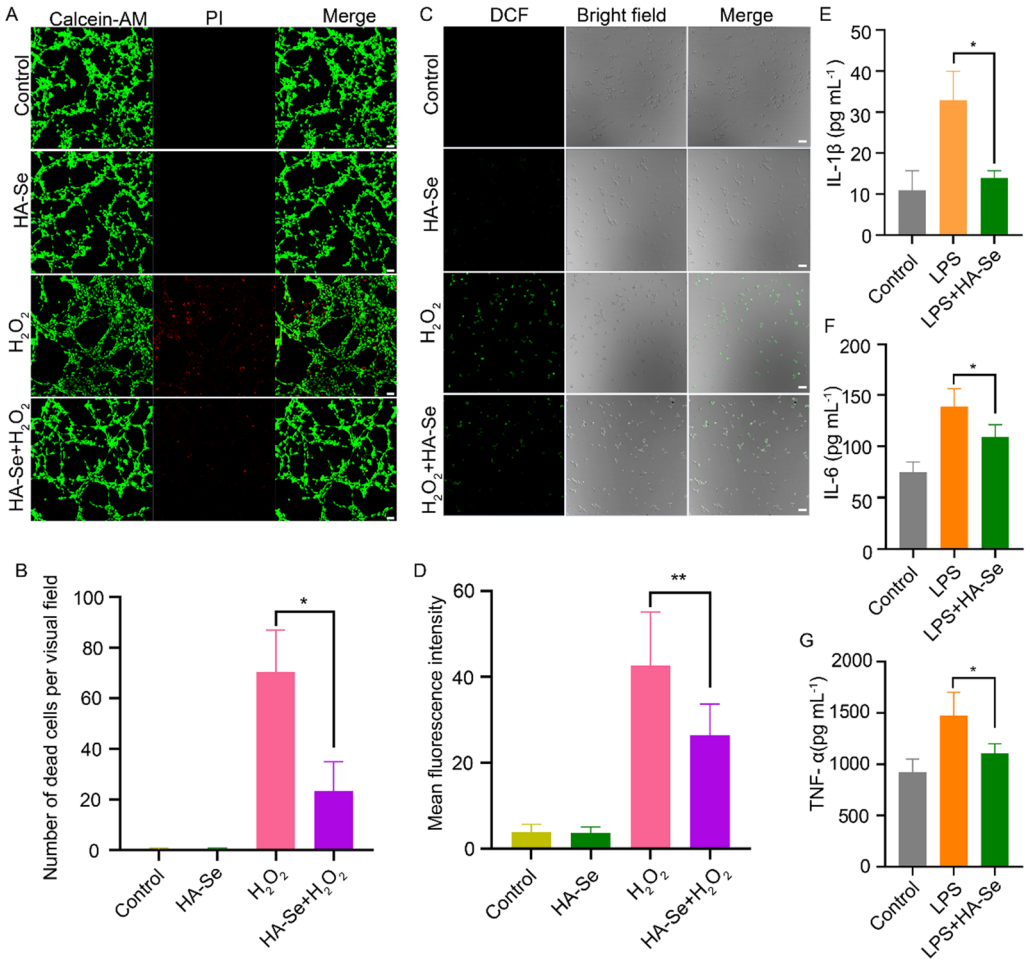

Fig. 2 The efficacy of HA-Se NPs in preventing H_2O_2-induced oxidative stress and inflammation was evaluated. **A** Live/dead staining of astrocytes. Scale bar = 20 μm. The concentration of H_2O_2 was 100 μM. **B** Quantitative analysis of astrocyte cell death. $^*P < 0.05$. **C** Levels of reactive oxygen species within astrocytes were determined via DCFH-DA staining. **D** Quantitative analysis of DCF fluorescence intensity in astrocytes. $^{**}P < 0.01$. Quantification of **E** interleukin (IL)-1β, **F** IL-6, and **G** tumor necrosis factor (TNF)-α levels in BV2 cell culture medium in the presence or absence of HA-Se NPs. $^*P < 0.05$

Figure S6A, B). Consistently, the presence of HA-Se NPs effectively reduced the amount of ROS during in vitro culture of astrocytes and PC12 cells, as indicated by the reduced fluorescence intensity of a ROS probe (Fig. 2C, D and Additional file 1: Figure S6C, D). The anti-inflammatory efficacy of HA-Se NPs was determined in BV2 cells exposed to LPS (1 μg/mL). Incubation with HA-Se NPs completely reversed the LPS-induced increase in primary cytokines (TNF-α, IL-1β, and IL-6) (Fig. 2E–G).

Targeting efficiency of HA-Se NPs in vitro and in vivo

Insufficient information exists regarding CD44 expression within the injured spinal cord [44]. Thus, we evaluated CD44 expression in the injured spinal cord of rats. Increases in CD44 levels were detected at 1-, 3-, 5-, and 7-days post-injury (Fig. 3A–C). To further characterize the cells which exhibited CD44 upregulation, we performed immunofluorescence staining. As indicated in Fig. 3D and E, GFAP and CD44 signals completely co-localized, while Iba-1 and CD44 exhibited partial co-localization. In addition, CD68 and CD44 fluorescence signals as well as those of NueN and CD44 exhibited incomplete colocalization (Fig. 3F and G). Taken together, these findings suggest that CD44 was expressed in astrocytes and a subset of microglial cells.

It has been previously established that an inflammatory microenvironment, such as that induced by LPS, promotes the secretion of proinflammatory cytokines by microglial cells and astrocytes [45–48]. Further, research has shown that is CD44 upregulated during the inflammatory response [49–51]. Thus, we exposed astrocytes to LPS for 24 h, observing notably enhanced CD44 expression in the LPS group as compared to controls, indicative of a substantial elevation in CD44 following LPS

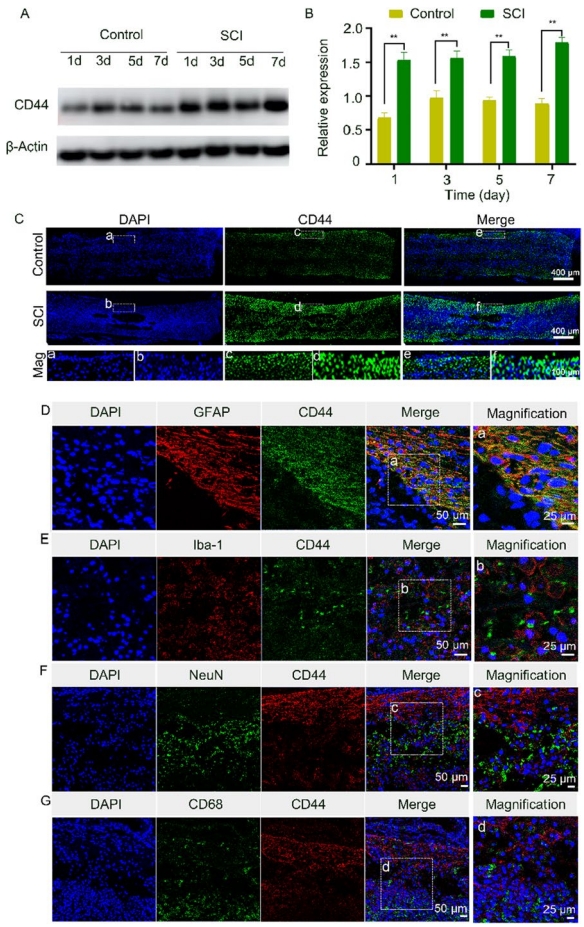

Fig. 3 CD44 expression in the injured spinal cord. **A** Representative western blot images of CD44 expression in the control and SCI groups. **B** Densitometric analysis of CD44 levels based on data in (**A**). $^{**}P < 0.01$ in comparison to the control group. **C** CD44 immunofluorescence staining of injured spinal cord samples. Mag: Magnification. **D** Immunofluorescence staining of injured spinal cord samples for GFAP (red) and CD44 (green). **E** Immunofluorescence staining of injured spinal cord samples for CD44 (green) and Iba-1 (red). **F** Immunofluorescence staining of injured spinal cord samples for NeuN (green) and CD44 (red). **G** Immunofluorescence staining of injured spinal cord samples for CD68 (green) and CD44 (red)

activation (Fig. 4A and Additional file 1: Figure S7). Western blotting confirmed the upregulation of CD44 in LPS-stimulated astrocytes (Additional file 1: Figure S8A, B). Conversely, the presence of glutamate did not alter CD44 expression in astrocytes, as indicated by the data presented in Additional file 1: Figure S8C and D.

Next, we explored the targeting efficiency of HA-Se NPs in vitro, using LPS to induce CD44 expression in astrocytes. The time-dependent internalization of HA-Se NPs by astrocytes was confirmed based on a gradual increase in red fluorescence, which we attributed to CD44 expression. To corroborate this observation, we blocked CD44 with HA [37, 52, 53]. In LPS-activated astrocytes, time-dependent internalization was observed in both the HA pretreatment and non-pretreatment groups, being stronger in the latter group during the initial 4 and 8 h (Fig. 4B and Additional file 1: Figure S9). These results validated that enhanced HA-Se NPs internalization was achieved via CD44. To assess NP targeting efficacy in vivo, rats were administered Cy5-labeled HA-Se NPs after SCI. Following injection, the injured spinal cord exhibited a high fluorescent signal within a mere 6-h window, with the fluorescent signal remaining strong at 12 h and subsequently waning at 24 h, possibly due to deterioration of the HA-Se NP shell structure. Cy5-labeled HA-Se NPs accumulated in the heart, liver, spleen, lungs, and kidneys, particularly in the liver and kidneys, which may suggest that the NPs are metabolized via these two organs (Fig. 4C). The fluorescence signal of the liver was gradually increased and reached to maximum at 12 h post-injection.

Neuroprotective activity of HA-Se NPs in vivo

To investigate the neuroprotective activity of HA-Se NPs in vivo, BBB scores were utilized to evaluate the restoration of locomotor function over a 12-week post-injury duration. The recovery of locomotor function was notably accelerated in all treatment groups as opposed to the saline group within a 12-week period following SCI. The group receiving 10 mg kg^{-1} exhibited a notably elevated BBB score compared to the other groups (Fig. 5A). This observation is also supported by visual inspection of SCI rat spinal cord tissues (Fig. 5B). Assessment of the pathological alterations that transpired at the site of the lesion revealed that the condition of spinal cords was notably inferior in the saline group, with greater numbers of inflammatory cells detected. In contrast, the animals receiving HA-Se NPs exhibited varying degrees of improvement in spinal cord integrity. Figure 5C illustrates that the animals receiving 10 mg/kg HA-Se NPs displayed the least extensive lesion cavity, with a sparse presence of inflammatory cells (Additional file 1: Figure S10). Based on the aforementioned observations, it can be inferred that the application of HA-Se NPs was effective in halting the progression of secondary injury cascades.

Axonal demyelination is a common result of SCI [6, 54, 55]. In light of this, we utilized LFB staining to assess the degree of myelination in axons. As indicated by Fig. 5D, there was a reduction in the number of intact myelin sheaths in the group treated with saline. HA-Se NPs treatment alleviated the severity of demyelination, indicating that HA-Se NPs preserved myelin sheaths following injury. To further verify changes in myelination, we performed TEM analysis of the myelin sheaths.

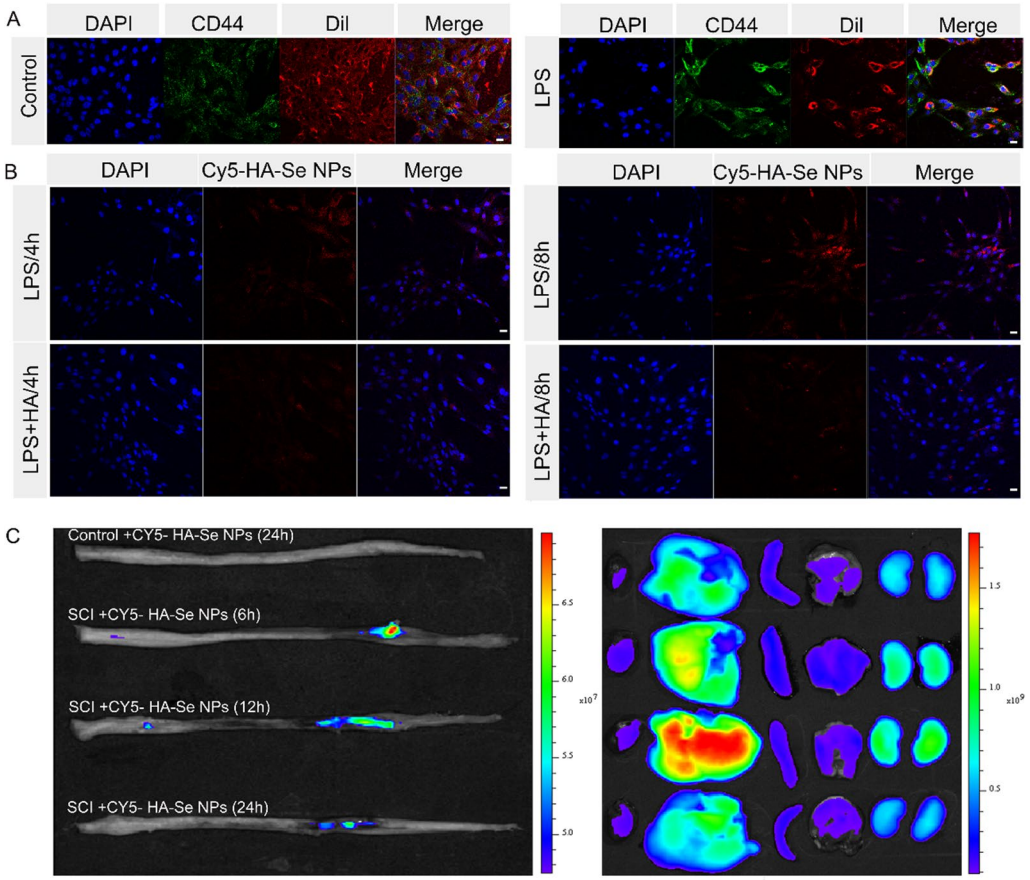

Fig. 4 CD44 immunofluorescence staining in astrocytes and internalization of Cy5-HA-Se NPs. **A** Astrocytes stained for CD44 and Dil. Scale bar = 50 μm. **B** Cy5-HA-Se NPs internalization by astrocytes after 4 and 8 h of incubation. Scale bar = 50 μm. **C** Targeting efficiency of HA-Se NPs in vivo. Fluorescence images of the major organs after intravenous injection of rats with Cy5-labeled HA-Se NPs. The organs were collected at 24 h post-injection from non-treated rats and at 6, 12, and 24 h post-injection from SCI rats

In the saline-treated group, TEM images indicated that the myelin sheaths were disorganized and not compactly arranged (Fig. 5E). Meanwhile, the group treated with HA-Se NPs demonstrated greater amount, size, and thickness of myelin sheaths, with the best outcomes observed in rats treated with 10 mg/kg of HA-Se NPs.

It is worth mentioning that the application of HA-Se NPs brought about a significant reduction in the levels of cleaved caspase-3, which were significantly elevated following SCI (Fig. 5F, G). Western blot confirmed the significant reduction in cleaved caspase-3 levels within the spinal cords of animals treated with HA-Se NPs in comparison to those treated with saline. Subsequently, we assessed the remedial impacts of HA-Se NPs on both neurons and axons. Saline-treated controls exhibited a substantial loss of axons and neurons, as observed via confocal imaging. Conversely, animals administered different concentrations of HA-Se NPs displayed greater myelin sheath and axon retention, which highlighted the protective potential of HA-Se NPs in the affected area (Fig. 6). This outcome is consistent with the observed improvement in locomotive function (Fig. 5A). In addition, a considerable number of CD68- and Iba-1-positive cells (macrophage/microglia) were observed at the injury site in the saline group. In comparison, the HA-Se NPs group exhibited a notable decrease in CD68- and Iba-1-positive cells (Additional file 1: Figure S11). Taken together, these observations supported the therapeutic value of HA-Se NPs in enhancing locomotor function recovery through the preservation of neurons and axons. It should also be noted that the major organs obtained from rats administered HA-Se NPs exhibited no visible alterations (Additional file 1: Figure S12). It can therefore be inferred that HA-Se NPs are safe and effective for the management of SCI.

Discussion

In the present study, we employed a facile redox approach to prepare the HA-Se NPs that specifically target CD44 receptor. HA-Se NPs scavenged ROS and restricted

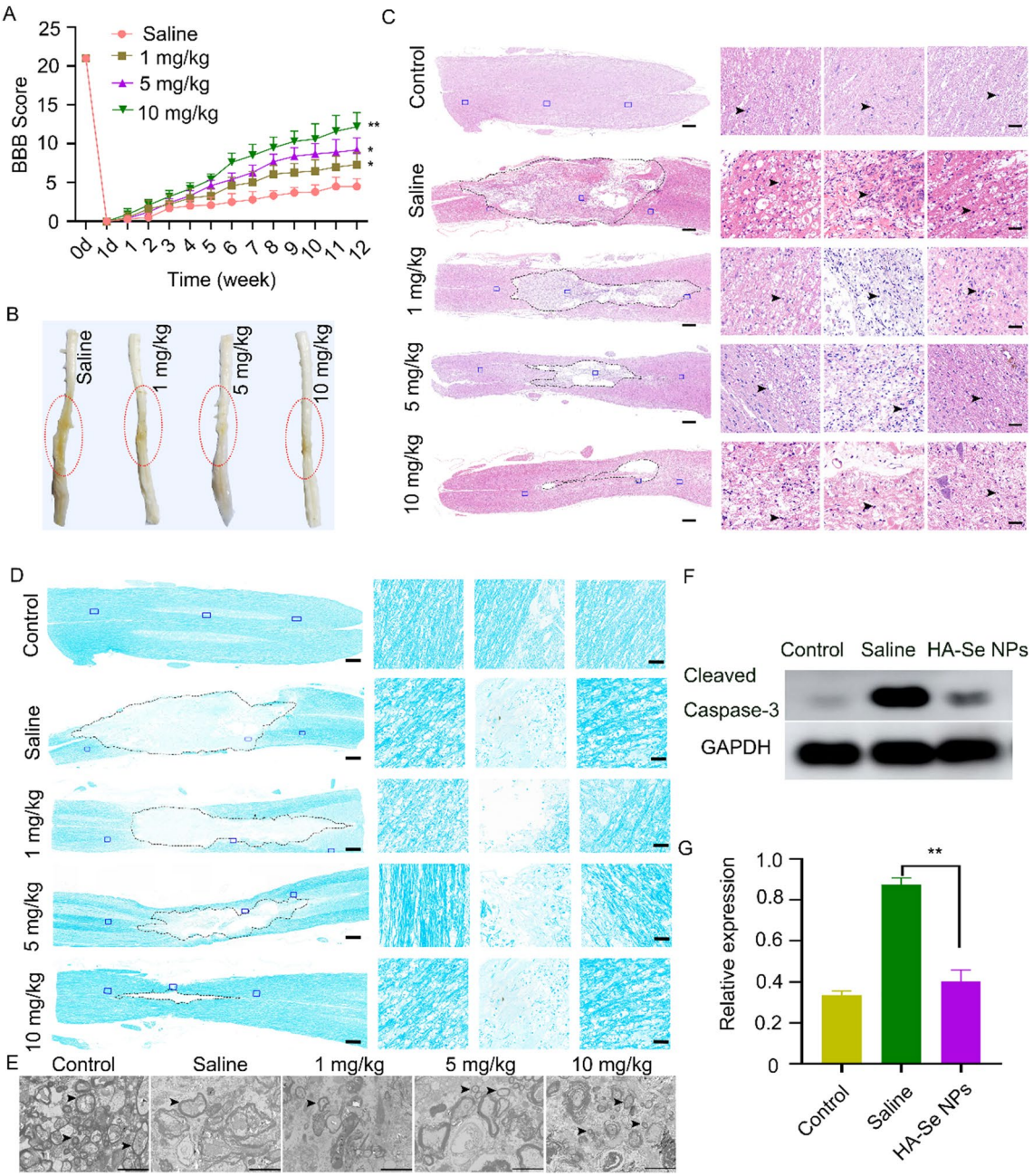

Fig. 5 Neuroprotective effects of HA-Se NPs. **A** Basso Beattie Bresnahan (BBB) scores of SCI rats. **B** Gross images of the spinal cord in different groups at 12 weeks post-injury. The lesion site is denoted by the red circle. **C** Images of hematoxylin and eosin (H&E) right, three magnified images of the areas marked by the blue squares. Scale bars = 500 and 50 μm, respectively. Dotted line and arrows indicate the lesion cavity and inflammatory cells, respectively. **D** Images of an injured spinal cord stained with LFB. Scale bars = 500 and 50 μm, respectively. Dotted line indicates the lesion cavity. **E** Representative TEM images of different experimental groups after treatment with saline or HA-Se NPs at the indicated concentrations. Scale bar = 2 μm. Arrows indicate myelin sheaths. **F** Western blot analysis of cleaved caspase-3 in injured spinal cord tissues 24 h after injury. GAPDH was used as the internal control. **G** Densitometric analysis of cleaved caspase-3 levels based on (D). $^{**}P < 0.01$ in relation to the saline group

inflammatory responses. Further, HA-Se NPs efficiently accumulated at lesions by targeting CD44. Consequently, HA-Se NPs protected axons and neurons within the injury site, improving functional recuperation in a rat model of SCI. Therefore, we believe that CD44-targeting HA-Se NPs represent a viable therapeutic option for the treatment of SCI.

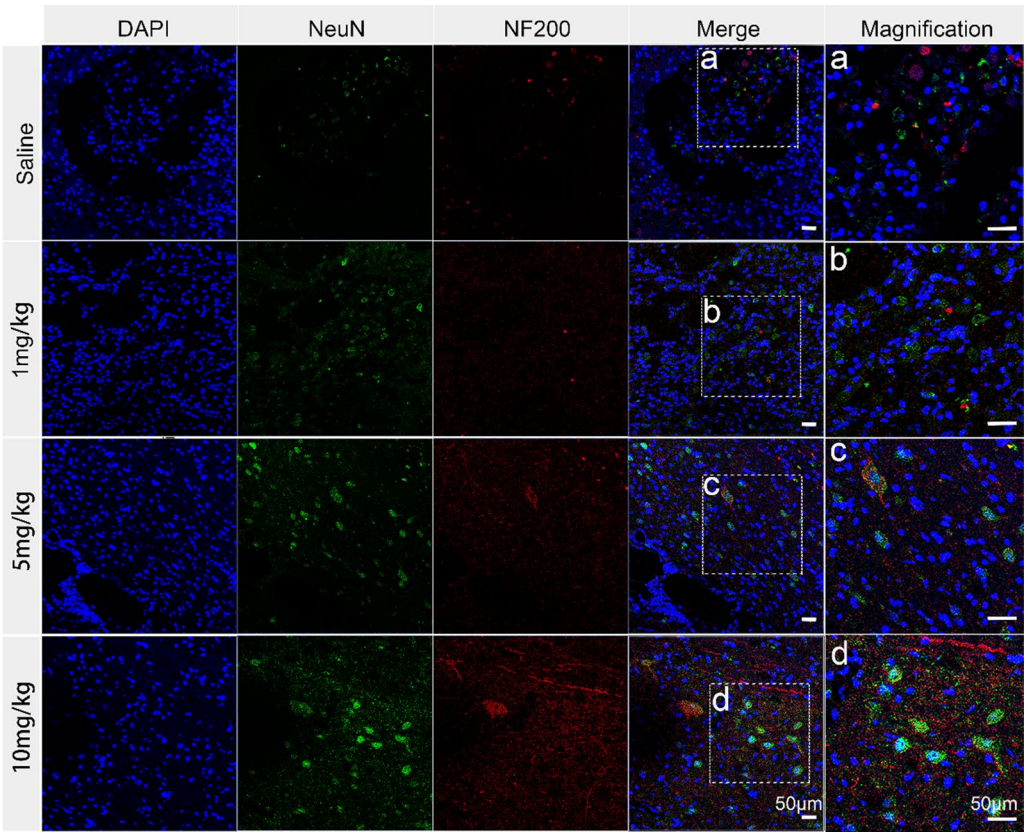

Fig. 6 Immunohistochemistry of scar tissue labeled with NeuN (green) and NF200 (red). The group that received a dosage of 10 mg/kg exhibited greater preservation of both neurons and axons within the affected spinal cord tissue, even at 12 weeks post-SCI. Scale bar = 50 μm

Therapeutic approaches that involve scavenging ROS and inhibiting inflammatory cascades within the damaged spinal cord have demonstrated efficacy in enhancing functional recovery following SCI [56, 57]. In the preliminary in vitro experiments, HA-Se NPs effectively scavenged DPPH free radicals, in a manner dependent on concentration and exposure time. To explore the capacity of HA-Se NPs for reducing ROS at the cellular level, H_2O_2 was used to mimic oxidative stress. HA-Se NPs significantly reduced ROS levels during in vitro culture of astrocytes and PC12 cells, in addition to reducing cell death. The damaged and surrounding spinal cord tissues are subject to infiltration by microglia/macrophages, which subsequently secrete proinflammatory cytokines, shaping a hostile microenvironment that hinders SCI repair [58–60]. Our results showed that HA-Se NPs dramatically suppress LPS-induced inflammatory cytokine (TNF-α, IL-1β, and IL-6) production. The anti-inflammatory capacity of HA-Se NPs was further demonstrated in our rat SCI model, based on a reduction in CD68- and Iba-1-positive cell infiltration. Taken together, these observations highlight the protective effect of HA-Se NPs, which shield spinal cord cells from oxidative stress-induced injury and aberrant inflammation.

Excessive ROS generation and the consequent aggressive inflammatory response are known to impede SCI repair [18]. Therefore, a prompt therapeutic intervention that involves the elimination of ROS and suppression of inflammation can yield substantial benefits in terms of sustained neurological and functional recovery [14]. In addition, targeting ability is an essential aspect in the enhanced curative effect and lesser side effects associated with NPs [61]. Our results showed that the CD44 receptor was highly expressed in astrocytes and microglia following SCI, in accordance with previous research [44, 62]. HA is a well-known ligand of the CD44 receptor [63]. Through series in vitro studies, we found that the HA-Se NPs were effectively internalized by astrocytes. In addition, the HA-Se NPs effectively accumulated within damaged spinal cord tissue, where they persist for a duration of 24 h. The positive impact of HA-Se NPs may be attributed to their exceptional targeting capability, which enables prolonged accumulation within spinal cord tissue.

Conclusions

Herein, we developed CD44-targeting HA-Se NPs for enhanced SCI recovery through ROS elimination and the suppression of inflammatory responses. Upon SCI, astrocytes and certain microglial cells exhibit upregulated CD44 expression, which facilitate the accumulation HA-Se NPs and consequent protection of axons and neurons within the injury site. The aforementioned observations underscore the auspicious therapeutic potential of HA-Se NPs in oxidative stress-induced disease or their viability as potential nanocarriers for the treatment of SCI.

Abbreviations

BBB	Basso Beattie Bresnahan
BSA	Bovine serum albumin
CLSM	Confocal laser-scanning microscope
DMEM	Dulbecco's modified Eagle's medium
LPS	Lipopolysaccharide
GFAP	Glial fibrillary acidic protein
H&E	Hematoxylin and eosin
HA	Hyaluronic acid
PBS	Phosphate-buffered saline
ROS	Reactive oxygen species
SCI	Spinal cord injury
SEM	Scanning electron microscopy
TEM	Transmission electron microscopy
NPs	Nanoparticles

Supplementary Information

The online version contains supplementary material available at https://doi.org/10.1186/s12951-024-02302-0.

Additional file 1: Figure S1. The stability of HA-Se NPs in pH 7.4 PBS buffer. **Figure S2.** Transmission electron microscopy (TEM) image of HA-Se NPs revealing a spherical shape, with a mean diameter of approximately 95 nm. **Figure S3.** X-ray photoelectron spectrum of hyaluronic acid-selenium nanoparticles (HA-Se NPs). **Figure S4.** *In vitro* biocompatibility of HA-Se NPs. Viability of PC12 cells and astrocytes incubated with different concentrations of HA-Se NPs for (A) 24 and (B) 48 h. Data are presented as mean ± SD ($n = 3$ for each group). **Figure S5.** The HA-Se nanoparticles scavenge reactive oxygen species (ROS) to protect astrocytes from oxidative damage. [H_2O_2] =100 μM. **Figure S6.** HA-Se NPs scavenge ROS to protect PC12 cells *in vitro*. (A) Live/dead staining of PC12 cells. Scale bar = 20 μm. (B) Quantitative analysis of dead cells. (C) Intracellular ROS levels in PC12 cells were measured using DCFH-DA staining. Scale bar = 20 μm. (D) Quantitative analysis of DCF fluorescence intensity in the cells. **P<0.01. **Figure S7.** Quantitative analysis of the mean fluorescence intensity of CD44 staining in Fig. 4A. **P<0.01 compared to the control group. **Figure S8.** Astrocytes overexpress CD44 upon LPS exposure. Western blot analysis of CD44 in astrocytes upon (A) LPS and (C) glutamate activation. (B, D) Densitometric analysis of CD44 levels based on the data in (A) and (C), respectively. *P<0.05, **P<0.01. **Figure S9.** Quantitative analysis of the mean fluorescence intensity of Cy5-HA-Se NPs in Fig. 4B. **P<0.01 in comparison to the LPS/8 h group. **Figure S10.** Quantitative analysis of inflammatory cells in Figure 5C,* P < 0.05, in the saline group compared with the 10 mg/kg group. **Figure S11.** Immunohistochemistry staining of scar tissue labeled with Iba-1 (green) and CD68 (red) 12 weeks after SCI. Scale bar = 50 μm. **Figure S12.** Hematoxylin & eosin (H&E) staining of the major organs in the experimental group. **Table S1.** Information on the antibodies used for immunofluorescence (IF) staining. **Table S2.** Antibodies used for western blotting (WB).

Acknowledgements

Not applicable.

Author contributions

WL: Conceptualization, Formal analysis, Writing-original draft and editing. YL: Conceptualization, Writing-review and editing. JZ: Formal analysis, Writing-review and editing. RN: Data curation, Writing-review and editing. CX: Writing-review and editing. MZ: Data curation. CX: Writing-review and editing, Funding acquisition. WL: Conceptualization, Writing-review and editing, Supervision, Funding acquisition. RG: Conceptualization, Funding acquisition, Writing review and editing, Supervision.

Funding

This work was supported by grants from the National Natural Science Foundation of China (grant number: 82271411, 51803072), Jilin Provincial Finance Program (Grant number: 2022SCZ10, 2022SCZ25, 2023SCZ41, and 2021SCZ07), Jilin Provincial Science and Technology Program (Grant number: YDZJ202201ZYTS038, 20200201341JC), Youth Support Programmed Project of China Japan Union Hospital of Jilin University(2022qnpy11).

Availability of data and materials

No datasets were generated or analysed during the current study.

Declarations

Ethics approval and consent to participate

All animal procedures were performed under the guidelines of the institutional review board and the ethics committee of Jilin University (approval No. SY202103013).

Consent for publication

Not applicable.

Competing interests

The authors declare no competing interests.

Received: 15 November 2023 Accepted: 13 January 2024
Published online: 23 January 2024

References

1. Ong W, Pinese C, Chew SY. Scaffold-mediated sequential drug/gene delivery to promote nerve regeneration and remyelination following traumatic nerve injuries. Adv Drug Deliv Rev. 2019;149–150:19–48. https://doi.org/10.1016/j.addr.2019.03.004.
2. Hutson TH, Di Giovanni S. The translational landscape in spinal cord injury: focus on neuroplasticity and regeneration. Nat Rev Neurol. 2019;15:732–45. https://doi.org/10.1038/s41582-019-0280-3.
3. Huang H, Young W, Skaper S, Chen L, Moviglia G, Saberi H, et al. Clinical neurorestorative therapeutic guidelines for spinal cord Injury (IANR/CANR version 2019). J Orthop Translat. 2020;20:14–24. https://doi.org/10.1016/j.jot.2019.10.006.
4. Silva NA, Sousa N, Reis RL, Salgado AJ. From basics to clinical: a comprehensive review on spinal cord injury. Prog Neurobiol. 2014;114:25–57. https://doi.org/10.1016/j.pneurobio.2013.11.002.
5. Li L, Xiao B, Mu J, Zhang Y, Zhang C, Cao H, et al. A MnO2 nanoparticle-dotted hydrogel promotes spinal cord repair via regulating reactive oxygen species microenvironment and synergizing with mesenchymal stem cells. ACS Nano. 2019;13:14283–93. https://doi.org/10.1021/acsnano.9b07598.
6. Ahuja CS, Wilson JR, Nori S, Kotter MRN, Druschel C, Curt A, et al. Traumatic spinal cord injury. Nat Rev Dis Primers. 2017;3:17018. https://doi.org/10.1038/nrdp.2017.18.
7. Führmann T, Anandakumaran PN, Shoichet MS. Combinatorial therapies after spinal cord injury: how can biomaterials help? Adv Healthc Mater. 2017;6: 1601130. https://doi.org/10.1002/adhm.201601130.

8. Wu W, Lee SY, Wu X, Tyler JY, Wang H, Ouyang Z, et al. Neuroprotective ferulic acid (FA)-glycol chitosan (GC) nanoparticles for functional restoration of traumatically injured spinal cord. Biomaterials. 2014;35:2355–64. https://doi.org/10.1016/j.biomaterials.2013.11.074.
9. Cerqueira SR, Oliveira JM, Silva NA, Leite-Almeida H, Ribeiro-Samy S, Almeida A, et al. Microglia response and in vivo therapeutic potential of methylprednisolone-loaded dendrimer nanoparticles in spinal cord injury. Small. 2013;9:738–49. https://doi.org/10.1002/smll.201201888.
10. Wang XJ, Shu GF, Xu XL, Peng CH, Lu CY, Cheng XY, et al. Combinational protective therapy for spinal cord injury medicated by sialic acid-driven and polyethylene glycol based micelles. Biomaterials. 2019;217: 119326. https://doi.org/10.1016/j.biomaterials.2019.119326.
11. Wang XJ, Peng CH, Zhang S, Xu XL, Shu GF, Qi J, et al. Polysialic-acid-based micelles promote neural regeneration in spinal cord injury therapy. Nano Lett. 2019;19:829–38. https://doi.org/10.1021/acs.nanolett.8b04020.
12. Shi Y, Kim S, Huff TB, Borgens RB, Park K, Shi R, et al. Effective repair of traumatically injured spinal cord by nanoscale block copolymer micelles. Nat Nanotechnol. 2010;5:80–7. https://doi.org/10.1038/nnano.2009.303.
13. Song YH, Agrawal NK, Griffin JM, Schmidt CE. Recent advances in nanotherapeutic strategies for spinal cord injury repair. Adv Drug Deliv Rev. 2019;148:38–59. https://doi.org/10.1016/j.addr.2018.12.011.
14. Andrabi SS, Yang J, Gao Y, Kuang Y, Labhasetwar V. Nanoparticles with antioxidant enzymes protect injured spinal cord from neuronal cell apoptosis by attenuating mitochondrial dysfunction. J Control Release. 2020;317:300–11. https://doi.org/10.1016/j.jconrel.2019.12.001.
15. Rao S, Lin Y, Du Y, He L, Huang G, Chen B, et al. Designing multifunctionalized selenium nanoparticles to reverse oxidative stress-induced spinal cord injury by attenuating ROS overproduction and mitochondria dysfunction. J Mater Chem B. 2019;7:2648–56. https://doi.org/10.1039/c8tb02520g.
16. Wang H, Lin F, Wu Y, Guo W, Chen X, Xiao C, et al. Carrier-free nanodrug based on co-assembly of methylprednisolone dimer and Rutin for combined treatment of spinal cord injury. ACS Nano. 2023;17:12176–87. https://doi.org/10.1021/acsnano.3c00360.
17. Nukolova NV, Aleksashkin AD, Abakumova TO, Morozova AY, Gubskiy IL, Kirzhanova EA, et al. Multilayer polyion complex nanoformulations of superoxide dismutase 1 for acute spinal cord injury. J Control Release. 2018;270:226–36. https://doi.org/10.1016/j.jconrel.2017.11.044.
18. Gao Y, Vijayaraghavalu S, Stees M, Kwon BK, Labhasetwar V. Evaluating accessibility of intravenously administered nanoparticles at the lesion site in rat and pig contusion models of spinal cord injury. J Control Release. 2019;302:160–8. https://doi.org/10.1016/j.jconrel.2019.03.026.
19. Mu X, He H, Wang J, Long W, Li Q, Liu H, et al. Carbogenic nanozyme with ultrahigh reactive nitrogen species selectivity for traumatic brain injury. Nano Lett. 2019;19:4527–34. https://doi.org/10.1021/acs.nanolett.9b01333.
20. Zhang T, Lin F, Liu W, Liu Y, Guo Z, Xiao C, et al. Reactive oxide species-scavenging lipid-polymer nanoparticles for neuroprotection after spinal cord injury. Appl Mater Today. 2021;24: 101109. https://doi.org/10.1016/j.apmt.2021.101109.
21. Thuret S, Moon LDF, Gage FH. Therapeutic interventions after spinal cord injury. Nat Rev Neurosci. 2006;7:628–43. https://doi.org/10.1038/nrn1955.
22. Luo W, Wang Y, Lin F, Liu Y, Gu R, Liu W, et al. Selenium-doped carbon quantum dots efficiently ameliorate secondary spinal cord injury via scavenging reactive oxygen species. Int J Nanomedicine. 2020;15:10113–25. https://doi.org/10.2147/IJN.S282985.
23. Jiang X, Liu X, Yu Q, Shen W, Mei X, Tian H, et al. Functional resveratrol-biodegradable manganese doped silica nanoparticles for the spinal cord injury treatment. Mater Today Bio. 2022;13: 100177. https://doi.org/10.1016/j.mtbio.2021.100177.
24. Kim JW, Mahapatra C, Hong JY, Kim MS, Leong KW, Kim HW, et al. Functional recovery of contused spinal cord in rat with the injection of optimal-dosed cerium oxide nanoparticles. Adv Sci (Weinh). 2017;4: 1700034. https://doi.org/10.1002/advs.201700034.
25. Gong W, Zhang T, Che M, Wang Y, He C, Liu L, et al. Recent advances in nanomaterials for the treatment of spinal cord injury. Mater Today Bio. 2023;18: 100524. https://doi.org/10.1016/j.mtbio.2022.100524.
26. Liu Y, Lin F, Zhang T, Wu C, Liu W, Wang H, et al. Toxic aldehyde-scavenging polypeptides mitigate secondary injury after spinal cord injury. Sci China Mater. 2023;66:2925–37. https://doi.org/10.1007/s40843-022-2409-4.
27. Zeng L, Chen J, Ji S, Chan L, Zheng W, Chen T. Construction of a cancer-targeted nanosystem as a payload of iron complexes to reverse cancer multidrug resistance. J Mater Chem B. 2015;3:4345–54. https://doi.org/10.1039/c4tb02010c.
28. Nagy G, Pinczes G, Pinter G, Pocsi I, Prokisch J, Banfalvi G. In situ electron microscopy of Lactomicroselenium particles in probiotic bacteria. Int J Mol Sci. 2016;17: 1047. https://doi.org/10.3390/ijms17071047.
29. Li Y, Li X, Wong YS, Chen T, Zhang H, Liu C, et al. The reversal of cisplatin-induced nephrotoxicity by selenium nanoparticles functionalized with 11-mercapto-1-undecanol by inhibition of ROS-mediated apoptosis. Biomaterials. 2011;32:9068–76. https://doi.org/10.1016/j.biomaterials.2011.08.001.
30. Xu C, Qiao L, Guo Y, Ma L, Cheng Y. Preparation, characteristics and antioxidant activity of polysaccharides and proteins-capped selenium nanoparticles synthesized by Lactobacillus casei ATCC 393. Carbohydr Polym. 2018;195:576–85. https://doi.org/10.1016/j.carbpol.2018.04.110.
31. Zhai X, Zhang C, Zhao G, Stoll S, Ren F, Leng X. Antioxidant capacities of the selenium nanoparticles stabilized by chitosan. J Nanobiotechnol. 2017;15: 4. https://doi.org/10.1186/s12951-016-0243-4.
32. Ferreira CA, Ni D, Rosenkrans ZT, Cai W. Scavenging of reactive oxygen and nitrogen species with nanomaterials. Nano Res. 2018;11:4955–84. https://doi.org/10.1007/s12274-018-2092-y.
33. Guo L, Xiao J, Liu H, Liu H. Selenium nanoparticles alleviate hyperlipidemia and vascular injury in ApoE-deficient mice by regulating cholesterol metabolism and reducing oxidative stress. Metallomics. 2020;12:204–17. https://doi.org/10.1039/c9mt00215d.
34. Cardoso R, Hare B, Lind DJ, McLean M, Volitakis CA, Laws I. The APOE ε4 allele is Associated with lower selenium levels in the brain: implications for Alzheimer's Disease. ACS Chem Neurosci. 2017;8:1459–64. https://doi.org/10.1021/acschemneuro.7b00014.
35. Ji Z, Zheng J, Ma Y, Lei H, Lin W, Huang J, et al. Emergency treatment and photoacoustic assessment of spinal cord injury using reversible dual-signal transform-based selenium antioxidant. Small. 2023;19: e2207888. https://doi.org/10.1002/smll.202207888.
36. Cong W, Bai R, Li YF, Wang L, Chen C. Selenium nanoparticles as an efficient nanomedicine for the therapy of Huntington's disease. ACS Appl Mater Interfaces. 2019;11:34725–35. https://doi.org/10.1021/acsami.9b12319.
37. Choi KY, Han HS, Lee ES, Shin JM, Almquist BD, Lee DS, et al. Hyaluronic acid-based activatable nanomaterials for stimuli-responsive imaging and therapeutics: beyond CD44-mediated drug delivery. Adv Mater. 2019;31: e1803549. https://doi.org/10.1002/adma.201803549.
38. Khaing ZZ, Milman BD, Vanscoy JE, Seidlits SK, Grill RJ, Schmidt CE. High molecular weight hyaluronic acid limits astrocyte activation and scar formation after spinal cord injury. J Neural Eng. 2011;8: 046033. https://doi.org/10.1088/1741-2560/8/4/046033.
39. Lin F, Liu Y, Luo W, Liu S, Wang Y, Gu R, et al. Minocycline-loaded poly(alpha-lipoic acid)-methylprednisolone prodrug nanoparticles for the combined anti-inflammatory treatment of spinal cord injury. Int J Nanomedicine. 2022;17:91–104. https://doi.org/10.2147/IJN.S344491.
40. Zhang Y, Wang J, Zhang L. Creation of highly stable selenium nanoparticles capped with hyperbranched polysaccharide in water. Langmuir. 2010;26:17617–23. https://doi.org/10.1021/la1033959.
41. Yang L, Conley BM, Cerqueira SR, Pongkulapa T, Wang S, Lee JK, et al. Effective modulation of CNS inhibitory microenvironment using bioinspired hybrid-nanoscaffold-based therapeutic interventions. Adv Mater. 2020;32: e2002578. https://doi.org/10.1002/adma.202002578.
42. Xiao L, Wei F, Zhou Y, Anderson GJ, Frazer DM, Lim YC, et al. Dihydrolipoic acid-gold nanoclusters regulate microglial polarization and have the potential to alter neurogenesis. Nano Lett. 2020;20:478–95. https://doi.org/10.1021/acs.nanolett.9b04216.
43. Wang J, Li D, Liang C, Wang C, Zhou X, Ying L, et al. Scar tissue-targeting polymer micelle for spinal cord injury treatment. Small. 2020;16: e1906415. https://doi.org/10.1002/smll.201906415.
44. Moon C, Heo S, Sim KB, Shin T. Upregulation of CD44 expression in the spinal cords of rats with clip compression injury. Neurosci Lett. 2004;367:133–6. https://doi.org/10.1016/j.neulet.2004.05.101.
45. Greenhalgh AD, David S, Bennett FC. Immune cell regulation of glia during CNS injury and disease. Nat Rev Neurosci. 2020;21:139–52. https://doi.org/10.1038/s41583-020-0263-9.

46. Liddelow SA, Guttenplan KA, Clarke LE, Bennett FC, Bohlen CJ, Schirmer L, et al. Neurotoxic reactive astrocytes are induced by activated microglia. Nature. 2017;541:481–7. https://doi.org/10.1038/nature21029.
47. Liddelow SA, Barres BA. Reactive astrocytes: production, function, and therapeutic potential. Immunity. 2017;46:957–67. https://doi.org/10.1016/j.immuni.2017.06.006.
48. Sofroniew MV. Astrocyte barriers to neurotoxic inflammation. Nat Rev Neurosci. 2015;16:249–63. https://doi.org/10.1038/nrn3898.
49. Solier S, Müller S, Cañeque T, Versini A, Mansart A, Sindikubwabo F, et al. A druggable copper-signaling pathway that drives inflammation. Nature. 2023;617:386–94. https://doi.org/10.1038/s41586-023-06017-4.
50. Ponta H, Sherman L, Herrlich PA. CD44: from adhesion molecules to signaling regulators. Nat Rev Mol Cell Biol. 2003;4:33–45. https://doi.org/10.1038/nrm1004.
51. Puré E, Cuff CA. A crucial role for CD44 in inflammation. Trends Mol Med. 2001;7:213–21. https://doi.org/10.1016/s1471-4914(01)01963-3.
52. Takasugi M, Firsanov D, Tombline G, Ning H, Ablaeva J, Seluanov A, et al. Naked mole-rat very-high-molecular-mass hyaluronan exhibits superior cytoprotective properties. Nat Commun. 2020;11:2376. https://doi.org/10.1038/s41467-020-16050-w.
53. Skandalis SS, Karalis T, Heldin P. Intracellular hyaluronan: importance for cellular functions. Semin Cancer Biol. 2020;62:20–30. https://doi.org/10.1016/j.semcancer.2019.07.002.
54. Floriddia EM, Lourenço T, Zhang S, van Bruggen D, Hilscher MM, Kukanja P, et al. Distinct oligodendrocyte populations have spatial preference and different responses to spinal cord injury. Nat Commun. 2020;11:5860. https://doi.org/10.1038/s41467-020-19453-x.
55. Cunha MI, Su M, Cantuti-Castelvetri L, Müller SA, Schifferer M, Djannatian M, et al. Pro-inflammatory activation following demyelination is required for myelin clearance and oligodendrogenesis. J Exp Med. 2020;217: e20191390. https://doi.org/10.1084/jem.20191390.
56. Rao S, Lin Y, Lin R, Liu J, Wang H, Hu W, et al. Traditional Chinese medicine active ingredients-based selenium nanoparticles regulate antioxidant selenoproteins for spinal cord injury treatment. J Nanobiotechnol. 2022;20:278. https://doi.org/10.1186/s12951-022-01490-x.
57. Lin S, Li D, Zhou Z, Xu C, Mei X, Tian H. Therapy of spinal cord injury by zinc modified gold nanoclusters via immune-suppressing strategies. J Nanobiotechnol. 2021;19:281. https://doi.org/10.1186/s12951-021-01035-8.
58. Xi K, Gu Y, Tang J, Chen H, Xu Y, Wu L, et al. Microenvironment-responsive immunoregulatory electrospun fibers for promoting nerve function recovery. Nat Commun. 2020;11:4504. https://doi.org/10.1038/s41467-020-18265-3.
59. Ma D, Zhao Y, Huang L, Xiao Z, Chen B, Shi Y, et al. A novel hydrogel-based treatment for complete transection spinal cord injury repair is driven by microglia/macrophages repopulation. Biomaterials. 2020;237: 119830. https://doi.org/10.1016/j.biomaterials.2020.119830.
60. Liu W, Xu B, Xue W, Yang B, Fan Y, Chen B, et al. A functional scaffold to promote the migration and neuronal differentiation of neural stem/progenitor cells for spinal cord injury repair. Biomaterials. 2020;243: 119941. https://doi.org/10.1016/j.biomaterials.2020.119941.
61. Stater EP, Sonay AY, Hart C, Grimm J. The ancillary effects of nanoparticles and their implications for nanomedicine. Nat Nanotechnol. 2021;16:1180–94. https://doi.org/10.1038/s41565-021-01017-9.
62. Matsumoto T, Imagama S, Hirano K, Ohgomori T, Natori T, Kobayashi K, et al. CD44 expression in astrocytes and microglia is associated with ALS progression in a mouse model. Neurosci Lett. 2012;520:115–20. https://doi.org/10.1016/j.neulet.2012.05.048.
63. Salathia S, Gigliobianco MR, Casadidio C, Di Martino P, Censi R. Hyaluronic acid-based nanosystems for CD44 mediated anti-inflammatory and antinociceptive activity. Int J Mol Sci. 2023;24: 7286. https://doi.org/10.3390/ijms24087286.

Publisher's Note